ENVIRONMENT AND CLIMATE 1994-1998

Climate Change and Sea Level

Final report on the contribution of the

Alfred-Wegener-Institut für Polar- und Meeresforschung
Bremerhaven, Germany (AWI)

carried out under

Contract No. ENV4-CT95-0124

by

Philippe Huybrechts, Christoph Mayer, Hans Oerter,
and Friedrich Jung-Rothenhäusler

Bremerhaven, March 1999

1. Introduction

The main objective of the AWI contribution to the Contract was the study of the ice dynamics and mass balance of the Greenland ice sheet. This research was effectuated within the framework of the response of the Greenland ice sheet to global change and the ensuing consequences for global sea level. In line with the Work Programme, these studies encompassed both field work and modeling.

The field work was performed on two outlet glaciers at the northeastern Greenland coast. Nioghalvfjerdsfjorden (79-degree-fjord) glacier and Storstrømmen were chosen because of their large discharge from the Greenland ice sheet and because of their relative accessibility for collecting field data.

The modeling was performed on both the regional and global scale. Using field data collected within the Contract, a flowline model was developed for Nioghalvfjerdsfjorden glacier and embedded in a three-dimensional thermomechanical model for the entire Greenland ice sheet. The three-dimensional model itself was upgraded by implementing new datasets and improved mass-balance treatments. Experiments were performed using output from the Hamburg ECHAM coupled atmospheric/ oceanic GCM to prescribe the surface climate during the next century.

These studies enabled to refine estimates of the past, present, and future contribution of the Greenland ice sheet to global sea-level changes and to improve the understanding of the role of ice dynamics in the ice sheet evolution.

2. Field studies on Nioghalvfjerdsfjorden glacier in NE Greenland

Nioghalvfjerdsfjorden glacier, at 79.5° N, drains about 8.4% of the area of the Greenland ice sheet. The glacier forms a floating ice tongue of roughly 70 km length and 20 km width. The recent calving flux is very small (Thomsen et al., 1997), and it is therefore assumed that most of the ice draining into the floating part is melted away from the underside of the glacier.

Field work on the glacier started in 1996 by Danish glaciologists from GEUS/ DPC/ DCRS (Thomsen et al., 1997) and was joined by the AWI glaciology group in 1997 and in 1998. The contribution of the AWI group consists of:

- seismic measurements to determine ice thickness and water depth over the floating part
- tilt meter measurements in the hinge zone and across a ridge in the marginal shear zone
- CTD profiling in front of the glacier front (underneath sea ice)
- CTD profiling underneath the glacier through a borehole
- water depth soundings and CTD-measurements across Dijmpna Sund
- GPS measurements.

Results of the 1997 field season have been compiled by Mayer et al. (in preparation).

The 1998 field season lasted from July 15th through August 24th including departure and arrival at Værløse, Denmark. The foggy weather conditions in the summer of 1998 were not favorable for glaciological field work. In total only on 9 days work, which depended on helicopter assistance, could be carried out on the ice.

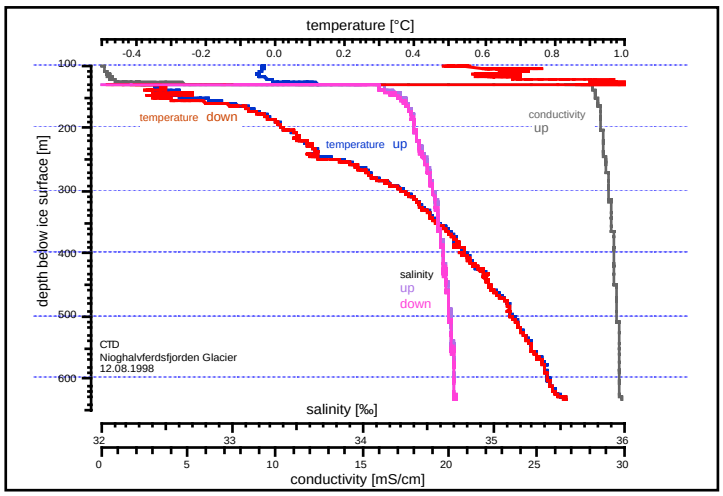

Figure 1: CTD profile obtained from a boreole at the GEUS Camp, Nioghalvfjerdsfjorden Glacier

Two additional seismic profiles were shot across the floating part of the glacier, one close to the grounding line area (7 shots) and the second profile (8 shots) half way in between the profiles of the 1997 season. The results improved the information about the sea bottom topography and solved some ambiguities in the hinge line area on whether the ice is floating or not. In general, the results from 1997, especially the steep flanks of the fjord as described by Mayer et al. (in preparation), were confirmed.

For the first time one CTD profile (Fig. 1) was measured through a borehole underneath the floating glacier (ice thickness 132 m) at the location of the GEUS ice camp down to a depth of 600 m below the ice surface (sea bottom appr. 930 m below ice surface). The borehole had been drilled by GEUS with a hot water drill. The distribution of temperature and salinity gives no strong indication for a thick fresh water layer underneath the glacier at this location, as it was found at the main glacier front (Mayer et al., in prep.).

In the outer part of Dijmpna Sund water depth soundings and 6 CTD measurements were done along a cross profile up to a distance of 5 km from the northern shore. The depth soundings yielded water depths up to 180 m. This means that the sound is deep enough for the water circulation to provide the energy for subglacial melting.

Special attention was given to one special feature on the glacier surface, a ridge zone parallel to the northern boundary of the fjord. In cooperation with GEUS, a strain net with 8 stakes was set up and stake movement measured by repeated GPS measurements. Combined with the stake net 6 tiltmeters were set up and tilting of the ice surface recorded over a period of 12 days (31.7.-11.8.98). In addition, ice thickness and water depth was measured by means of seismics (7 shots). The results show that the ridge is formed by shear stress at the boundary between floating and grounded parts of the ice stream. The tiltmeter measurements showed tidal movement of the ice where the seismics indicated floated ice and vanishing of the tidal influence where the ice is grounded.

3. Field studies on Storstrømmen glacier

The Storstrømmen glacier, in the hinterland of the meteorological station of Danmarkshavn (77° N) was already the objective of several glaciological investigations (Bøggild et al., 1994; Reeh et al., 1994). This glacier drains about 2% of the area of the Greenland ice sheet and, today, ends in a floating calving front, only a few kilometers long. This glacier is characterised by surging behaviour with a period of about 80 years (Jung-Rothenhäusler, 1998).

Only on 21-22 August 1997, that is after a period of two years, we were able to revisit the Storstrømmen Glacier after finishing the field work on Nioghalvsfjerdsfjorden glacier at the end of the ablation season. Two main objectives had been defined. First, the meteorological instrumentation should be recovered and the collected data be saved. Second, all stakes (Fig. 2) should be revisited and their height above the glacier surface and stake velocity determined.

Unfortunately, because of the overall low annual precipitation (Jung-Rothenhäusler et al., submitted) in northeastern Greenland as compared to the high ablation rates, the life span of stakes does not exceed more than three years. Hence most of the stakes used in the previous seasons had been melted out and were thus not relocatable. Just the stakes 08, 09 and 25 were found to be still standing. At the glacier front stakes 9225, 9330 and 9335 were melted out completely, but could be found. All other stakes were lost.

Hence velocity determinations were only possible on the three remaining stakes, as shown in Table 1. The results show that the overall flow pattern is still governed by the post-surge behaviour as shown in Jung-Rothenhäusler (1998). That is, very minimal flow rates at the glacier front but still considerable ice movement further up (stake 8,9). Hence the thickening process of the upper half of the glacier terminus is probably still continuing.

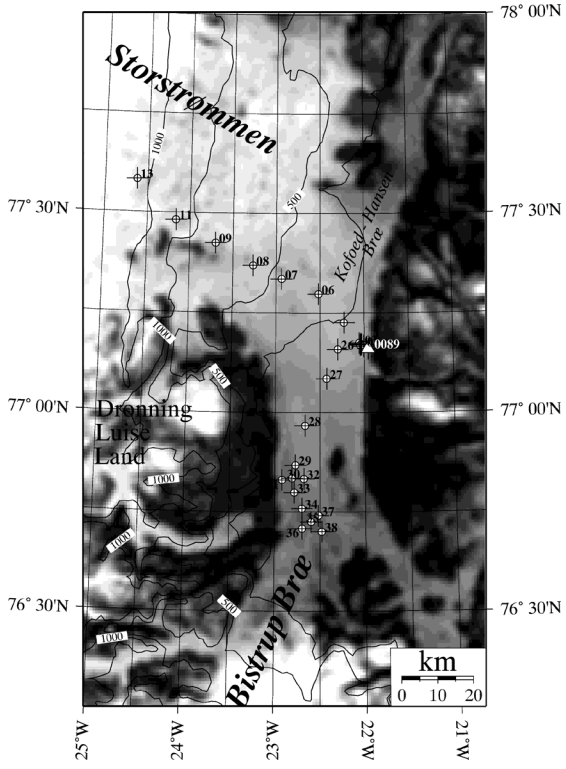

Figure 2: Map of Storstrømmen Glacier showing the positions of the stakes.

Stake	Position (WGS84)	Flow velocity (95-97) (m/y)	Flow direction (azimuth)
08	23°14'33.08" W 77°21'47.94" N 552 m	232	140°
09	23°41'02.99" W 77°25'05.84" N 631 m	232	153°
25	22°29'50.78" W 77°13'30.04" N 311 m	20	not determined

Table 1: Stake measurements on Storstrømmen between 1995 and 1997.

4. Detailed model study of a Northeast Greenland outlet glacier

4.1. Formulation and testing the physics of the flowline model

Most of the ice transport from the Greenland ice sheet towards the coast occurs in outlet glaciers, which are not well resolved on the 20 km grid of the 3-D ice sheet model. Therefore, an attempt was undertaken to relate the large-scale ice-sheet flow to the small-scale flow in outlet glaciers, using a glacier in Northeast Greenland as an example. Especially the glaciers of northern Greenland terminate as floating tongues, rather than ending in a grounded zone of intensive net melting. That makes it necessary to consider the transition of the flow regimes from grounded to floating ice.

For high-resolution simulations of the glacier dynamics, a flowline model was derived from a three-dimensional model that was developed to study the dynamics of the transition zone between an ice sheet and an ice shelf (Mayer, 1996). Specific to this model is that the full Stokes equations are considered and that no simplifications are made in the force balance. Unless more optimization work has been done, this three-dimensional model is too time consuming to be used for detailed simulations of ice sheets. The model is however much more efficient in two dimensions for calculating the ice flow in a vertical plane along an ice stream. Because there are no a priori differences in handling the physics of grounded and floating ice, transition effects and bridging forces can occur depending on the boundary conditions.

The mechanical part of the model has been applied to the EISMINT grounding line experiment (Huybrechts, 1997) and compared with other existing models. Calculation times have been greatly reduced by the conversion to two dimensions and by implementing a more efficient numerical scheme. Also, a more efficient handling of the subroutines, memory allocation and unrolling of loops resulted in a considerable speed-up of the model.

As further developments, thermomechnical coupling and parameterized surface mass balance along the lines of Huybrechts (1996) were implemented in the model. This allows to calculate the temperature distribution within the ice, depending on surface temperature, geothermal heat flux, heat advection and heat generation by basal shearing. The surface mass balance components, snow accumulation and meltwater run-off, are parameterized by a degree-day model according to the surface temperature.

For the understanding of mass flux and flow dynamics it is also necessary to consider probably extensive areas with basal sliding within the numerical simulations. For this purpose a Weertman-type sliding law was implemented in the model, which is applied in dependence of the basal temperature and the hydrostatic pressure at the glacier bed.
In an outlet glacier the ice flow usually shows different zones of lateral compression or extension. To account for this effect, flow band variations were introduced in the model, by deriving a transversal stress from the flowband width gradients.

This final, integrated model was tested on theoretical flowline geometries for sensibility of the different mechanisms implemented. Even with more modules running, the speed-up compared with the original mechanical flowline model for 187 by 9 gridpoints was by a factor of more than 100.

4.2. Incorporation of the field data in the numerical model

The flowline selection was made within a Greenland GIS, which is located at the AWI glaciology group and contains the most recent datasets available for Greenland (Jung-Rothenhäusler, 1998; Ekholm, 1996). Bedrock elevation, recent ice thickness and annual precipitation were also derived from this GIS dataset, including a revised precipitation distribution over North Greenland from AWI traverse data (Jung-Rothenhäusler et al., submitted). In addition to this data, results from the joint AWI/ GEUS/ DCRS/ DPC expedition were used for the construction of the flowline geometry. The most important information used as model input was the bedrock elevation calculated from the seismic measurements, because bedrock data were sparse over the ice sheet and totally missing on the floating part of the glacier until our recent field measurements. In addition, the ice thickness data along the central seismic profile on the floating glacier were used to extend the flowline from the grounding line to the coast.

The most significant climate-induced changes in the dynamics of the ice sheet can be expected in the parts with highest velocities close to the margin, where the mechanism of ice discharge can change from melting to calving. In order to reduce computing time, the considered flowline for the numerical simulations does not start at the ice divide, but at the 2000 m elevation isoline. For this region, also new radio echo sounding data will be available soon, which are anticipated to improve the grounded part of the bedrock elevation.

The combination of bedrock elevation and ice thickness data resulted in a flowline geometry starting at a surface elevation of 2000 m down to the calving front (Fig. 3, upper panel). In total, this flowline is 374 km long. A maximum ice thickness of 1700 m can be found at the upstream end of the flow section, where the bedrock elevation is 300 m. 125 km downhill the bedrock elevation drops below sea level for the current ice load. The lowest point at 900m b.s.l. is reached underneath the floating part, close to the calving front. The ice thickness change is rather smooth for the first 240 km. From there the ice thickness changes within 40 km from 1200 m to 700 m over a local bedrock high, before it reduces to 300 m just a few kilometers from the grounding line on the floating part. We still believe that this bedrock high and the connected strong ice thickness gradient is local and therefore removed it from the bedrock profile used for modelling. Also, the bedrock was smoothed for use in the model.

For implementation in the numerical model the geometry was gridded with a 2 km horizontal spacing between the grid points. In the vertical the resolution is 9 grid points in scaled coordinates. The original ice thickness distribution, ice velocities and calculated melt rates for the floating part were used as control for the setup of the parameters in the numerical model.

4.3. Linking the flowline model and the 3D model

Results from the 3-D model (§5) are used to prescibe boundary conditions at the upper end of the flowline. This point was chosen about 300 km inland from the grounding line at a position of 77.66°N and 32.12°W. This position is far enough from the grounding line to safely assume that longitudinal stresses are of minor importance for the ice flow. In this way, expensive calculations

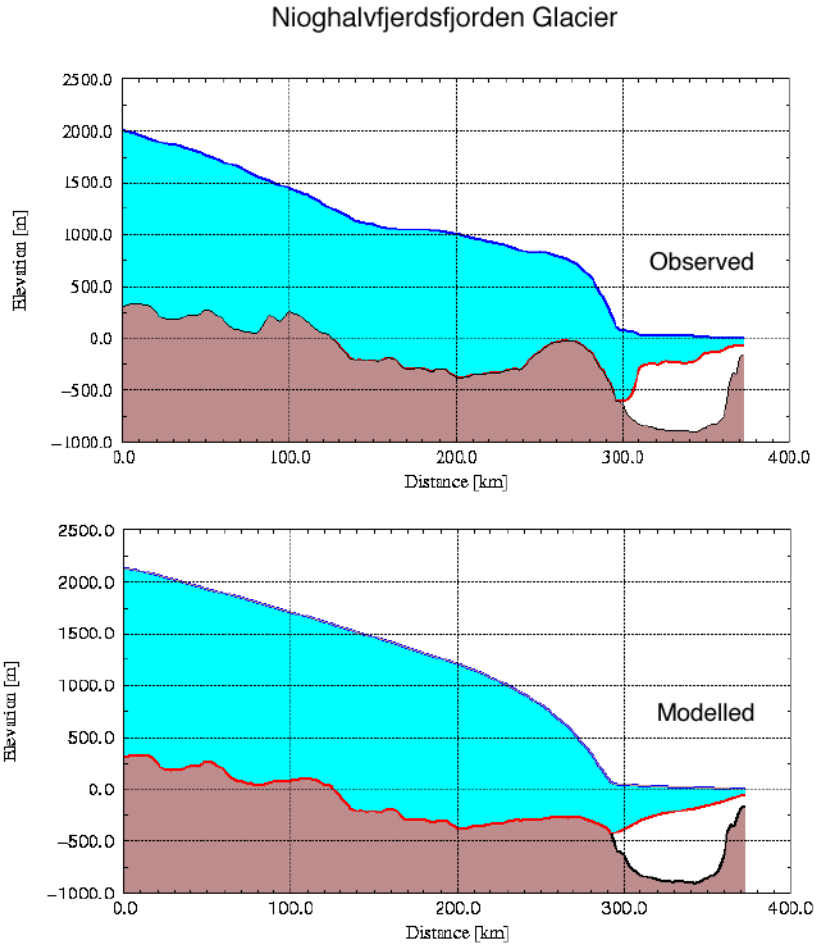

Figure 3: Geometry of the flowline feeding Nioghalvfjerdsfjorden glacier. The upper panel shows the observations, the lower panel is for a model run under steady state conditions.

with the flowline model up to the ice divide can be avoided and the flowline is able to take into account ice-sheet changes resulting from 3-D effects. The assumption is that the position of the flowline within the ice sheet remains constant in time, which is believed to approximately hold unless the ice sheet drastically changes its dimensions, for instance during a decay. Starting values for ice thickness, surface slope and ice velocities were interpolated to its exact position within a gridcell from the surrounding four corner points.

At this stage, output from the 3-D model was derived from a steady-state interglacial run. In comparison with the field data, the ice thickness from the 3-D model turned out to be 130 m higher. An important objective was to investigate whether the coupling of the two models would be able to yield physically and numerically sound results.

4.4. Results from the flowline model

In order to obtain a steady state profile close to the observations, several parameters had to be adjusted. The degree day factors for the calculation of the annual accummulation were the same than the ones used in the 3-D model (0.004 for snow and 0.0085 for ice of mm/y/PDD of ice equivalent). The calculated equilibrium line altitude using these factors is somewhat higher than 1100m. Even with very soft ice, the flow across the bedrock high close to the grounding line could not be realised in the model. It seems that this bedrock high does not represent a continuous barrier across the entire entrance of the glacier, but rather is a local feature which was subsequently removed from the profile.

Model calculations show that for a wide variety of temperature scenarios the basal temperature of the ice sheet in most of the drainage area of Nioghalvfjerdsfjorden is at the basal melting point (Huybrechts, 1996). The thermodynamical coupling of the model is not yet well tested. Therefore for the first steady-state calculations an idealized temperature profile was used, assuming the basal temperature to be at the pressure melting point everywhere. The surface temperature was calculated from the surface elevation and the geographical latitude. The upper 50% of the ice column was assumed to be isothermal, whereas in the lower half the temperature rises according to a 3rd degree polynome to the pressure melting point (Mayer and Huybrechts, in press).

No difference was made so far between Holocene and Wisconsin ice, but it was necessary to use an enhancement factor of 2.5 to obtain realistic flow velocities. For the same reason, also the basal sliding coefficient had to be increased by a factor 3 on the outermost 150 km of the grounded flow section. Steady state was reached after 16000 years. The resulting geometry is shown in Fig. 3 (lower panel). The most remarkable difference between the observations and the model result is the depression around kilometer 150. There are several possible explanations for this mismatch. The ice sheet could not be in steady state because of ongoing adjustments to past climatic changes. Alternatively, the flowline was not determined properly in this area, or changing basal sliding conditions could lead to stronger thinning around kilometer 110. Further work has to be done to decide which of these explanations influences this area most.

To obtain the observed ice shelf dynamics, basal melting had to be introduced in the model. The resulting melt rates (Fig. 4), with maximum values of 25 m/y close to the grounding line match very well with the melt rates calculated from field data.

The main results for the horizontal velocity profile demonstrates that the coupling did not introduce unwanted numerical effects or discontinuities. The horizontal velocity is very low in the grounded ice, but increases rapidly in the transition zone (Fig. 5). The width of this transition zone is of the order of four to five kilometers and thus agrees well with the assumption of a transition zone width of the order of ten times the ice thickness (Mayer and Huybrechts, in press). This model result shows that the flowline model is in agreement with the 3-D model and can be used for further investigations of the sensitivity of this specific area to climatic changes.

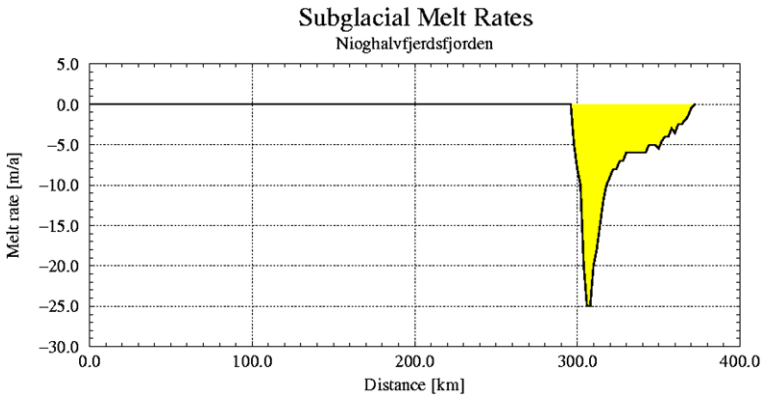

Figure 4: Basal melting rates along the Nioghalvfjerdsfjorden flowline which needed to be introduced to match the modelled position of the grounding line with the observed one.

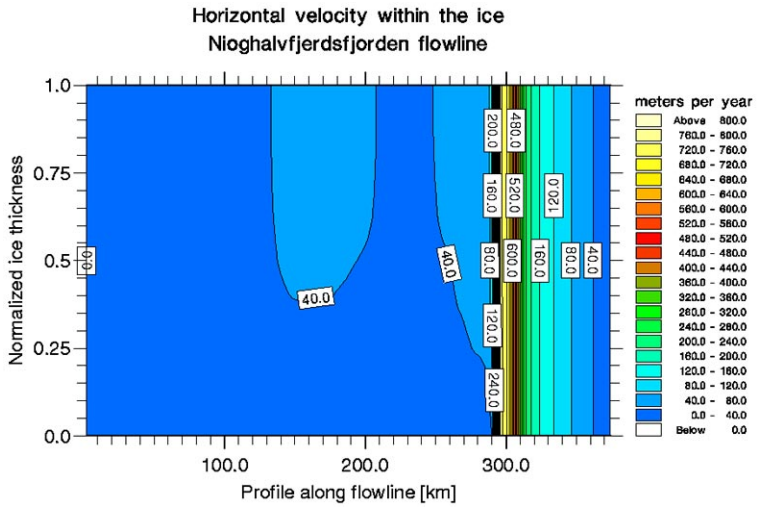

Figure 5: Horizontal velocity component in a vertical transect along the Nioghalvfjerdsfjorden flowline.

5. 3-D model studies on Greenland

The Greenland ice-sheet model used in this study corresponds to the version described in the appended paper (Huybrechts and de Wolde, in press). The ice-dynamics part distinguishes between grounded ice flow resulting from internal deformation and from basal sliding. The softness parameter of ice, which determines the rate of deformation, is a function of both the ice temperature and the age of the ice. For that reason, the three-dimensional velocity and temperature fields are calculated in the coupled mode and there is a rigorous tracking of particle trajectories. Isostatic compensation to the changing ice loading is treated by assuming local hydrostatic equilibrium and a viscous asthenosphere.

The model is externally forced by both eustatic sea level, which determines the coast line, and a temperature forcing, from which the surface boundary conditions are calculated. The mass-balance model distinguishes between snow accumulation, rainfall, superimposed ice formation, and runoff, which components are all parameterised in terms of temperature. Calving dynamics are not described explicitly. Instead, the contemporaneous coastline acts as a natural barrier to grounded ice, beyond which all ice is removed as calf ice. The main outputs of the model are the 3-D ice-sheet

geometry and a series of physical characteristics linked to the coupled velocity and temperature fields.

The model has been rigorously tested within the framework of the EISMINT intercomparison project (Huybrechts et al., 1996) and was used previously to investigate the Greenland ice sheet on time scales ranging from ice-sheet inception during the Tertiary, behaviour during the glacial cycles, and the response to future greenhouse warming.

5.1. Updating of Greenland datasets

The main inputs to the 3-D model are bed topography, a mask specifying the coastline, mean annual surface temperature and the mass balance (snow accumulation minus run-off). The horizontal resolution of the model is 20 km, resulting in a grid of 83 x 141 = 11703 gridpoints. So far, the bedrock topography was derived from the ETOPO5 dataset for the ice-free area, and from radio-echo soundings made by the Technical University of Denmark during airborne campaigns in

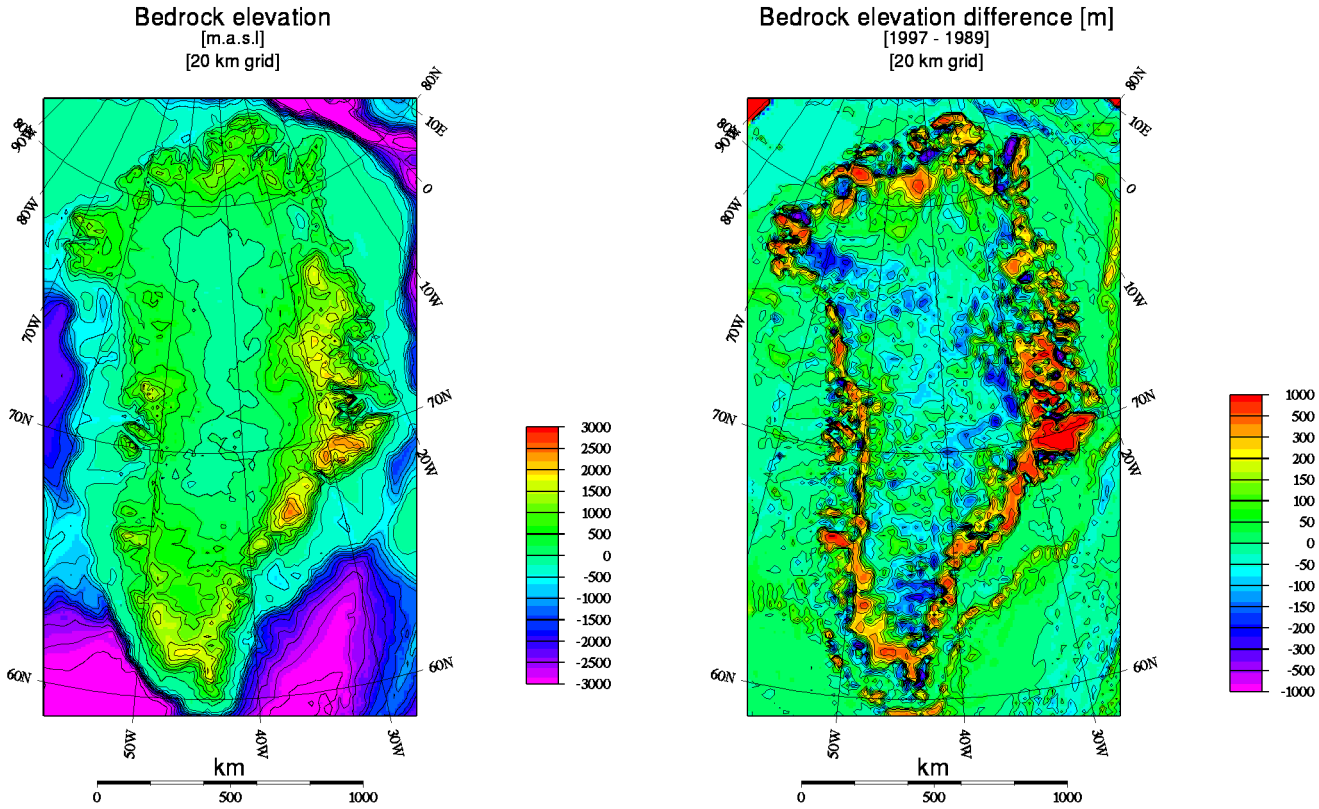

Figure 6: New dataset for bedrock topography (left panel). These data were derived by subtracting the most recent compilation of ice thickness data from the best surface elevation model derived from ERS-1 satellite altimetry. The topography of the ocean bottom was derived from the ETOPO5 dataset. Changes with respect to the older dataset (right panel) are largest near the ice margin, which is important to better represent ablation and runoff.

the seventies. The absolute elevation of the surface was calculated from the airplane's pressure altimeter along the same flight tracks (Letreguilly et al., 1991). However, these measurements had an uncertainty of about 140 m. In the mean time, much more precise surface elevation data have become available from satellite altimetry (Ekholm, 1996). The most recent data on a 1.2' x 3' resolution have been used to produce much more accurate datasets for the surface and bedrock

topography of the ice sheet. An example of the resulting bedrock topography and the differences with respect to the older dataset is displayed in Fig. 6.

The precipitation dataset used in previous calculations was digitized from a map presented in Ohmura and Reeh (1991). Also here, much more detailed information has been recently obtained from oversnow traverses, notably by the Alfred-Wegener-Institute. These new data have been embedded in the old Ohmura-Reeh datasets to produce new maps for accumulation and precipitation rate (Jung-Rothenhäusler et al., submitted), and were also interpolated on the model's 20 km grid. The new data show substantially drier conditions over North and Northeast Greenland. This is important for, amongst other things, the ice sheet's mass balance and the delineation of zones of basal melting and basal sliding.

For the interpolation of the irregularly spaced data points onto the regular model grid, extensive use was made of the continuous curvature spline algorithm 'surface' with a tension factor of zero, which is available as part of the GMT software (Smith and Wessel, 1990).

		old 1989 dataset 20 km (83 x 141)	new 1997 dataset 20 km (83 x 141)	new 1997 dataset 2.5 km (657 x 1121)
Land area	[km^2]	2187470	2187554	2167263
Ice sheet area	[km^2]	1673466	1612132	1577765
Ice volume	[km^3]	2845522	2775065	2775267
Total precipitation over ice sheet	[km^3 w.e]	538.665	505.258	493.054
Mean ice thickness	[m]	1700.376	1721.363	1758.986
Mean bedrock elevation of total Greenland	[m]	410.843	489.202	497.383
Mean surface elevation of ice sheet	[m]	2128.498	2166.219	2195.047
Mean precipitation rate over ice sheet	[mm w.e]	321.885	313.410	312.5014

Table 2: A comparison of ice sheet statistics derived from the old 1989 datasets (Letreguilly et al., 1991) and from the new datasets which were developed within the Contract. All averages are corrected for areal distortions of the map projection. The numbers represent new estimates of the physical characteristics of the Greenland ice sheet. The lower ice volume and ice sheet area obtained for the 1997 data is in part because small ice caps and glaciers have been excluded.

5.2. Improving the mass-balance treatment

The mass-balance model, yielding the local difference between snow accumulation and meltwater runoff, is essential for driving the Greenland ice sheet model. Besides the implementation of new datasets, the following improvements were made with respect to the mass-balance parameterisation described in Huybrechts et al. (1991):

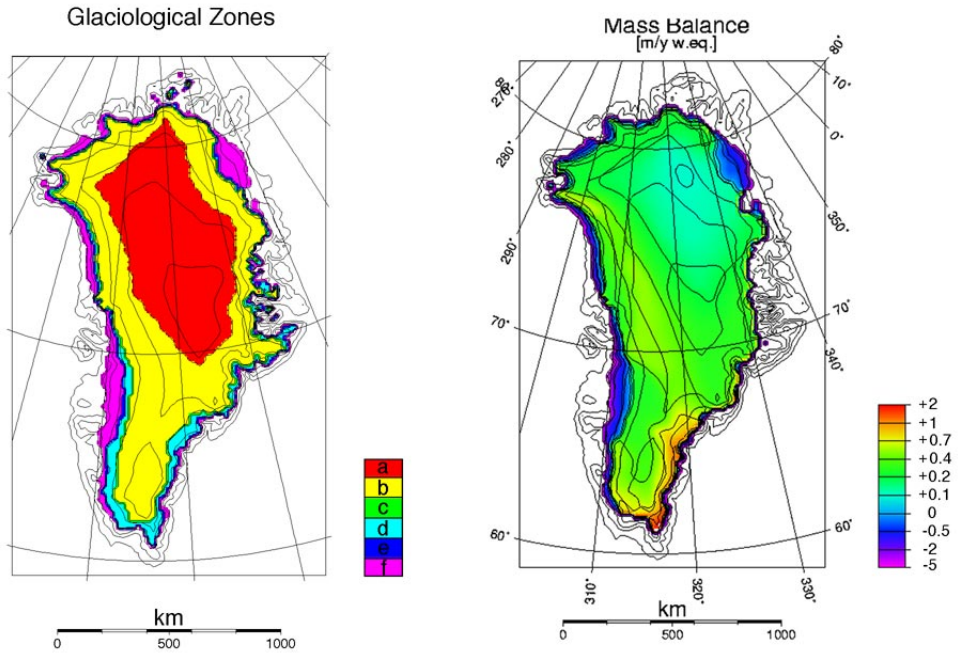

Figure 7: Characteristics of the surface mass-balance of the Greenland ice sheet. The left panel displays the predicted zonation (facies) of the Greenland ice sheet. a = dry snow zone; b = percolation zone; c = wet snow zone; d = slush zone; e = superimposed ice zone; f = ablation zone. The right panel shows the corresponding surface mass balance values for the main ice sheet only.

- The sum of Positive Degree Days used for calculating the snow- and ice melt are now derived in an exact analytical way using the mathematical properties of the standard normal density and distribution functions or are approached by a double exponential function.
- The model calculates the fraction of precipitation falling as rain depending on surface temperature and treats the rainwater in a similar fashion as the meltwater.
- Different alternatives are included to model the refreezing of melt- and rainwater in the firn. A detailed method taking into account water filling the firn pore (residual water) from Pfeffer et al. (1991) seemed to perform best.
- Detailed output was generated for each of the steps in the mass-balance calculation (fraction of rain, the maximal retarded snowmelt fraction, the expected positive degree days, the remaining snowcover and superimposed ice, the amount of melted old ice, runoff, the mass-balance, type of glaciological zone, etc.) for each geographical region and drainage area of the ice sheet to enable comparison with field measurements.

A new reference run was established by fine-tuning the parameters and compare the results with a compilation of available field data (mass-balance profiles, ELA, estimates of calf-ice production, etc.). In this run, the total accumulation over the ice sheet was calculated to be 505.26 km^3/y of water equivalent, the runoff 239.19 km^3/y and the residual amount of ice being discharged into the ocean 266.07 km^3/y (assuming a steady state). Figure 7 shows some of the characteristics of this standard run.

5.3. Greenhouse warming simulations

5.3.1. Initializing the current state

Because of the long response time scales of the Greenland ice sheet (of the order of thousands of years), it is unlikely that the ice sheet would have adjusted completely to its past climatic history.

This inertia is caused by such processes such as isostasy, thermomechanical coupling, reaction to surface mass-balance changes, and the advection of ice with different rheological properties in the basal shear layers (Huybrechts, 1994). To correctly assess the future response of the Greenland ice sheet, it is therefore necessary to start the calculations early enough in the past. Here, the current evolution of the Greenland ice sheet was obtained by initialising the calculations over the last two glacial cycles.

To that end, the model was forced over the last 225000 years by prescribing a uniform temperature change derived from the GRIP $\delta^{18}O$ record and imposing a sea-level history derived from the SPECMAP stack at a 100-year resolution. More details of this simulation can be found in the appended manuscript (Huybrechts and de Wolde, in press). The main result is that the Greenland ice sheet is currently close to a stationary state, corresponding to a sea-level change of only a few mm over the last century. However, the geographical pattern of ice-thickness evolution revealed a clear distinction between a thickening of between 0 and 20 mm/y over the accumulation zone and thinning rates locally in excess of 100 mm/y at the southwestern and northeastern margin of the ice sheet. Similar evolution patterns were also obtained in recent simulations in which the ice-sheet model was coupled with a sophisticated visco-elastic bedrock model (Le Meur and Huybrechts, 1998; Huybrechts and Le Meur, submitted; Le Meur and Huybrechts, submitted).

5.3.2. Downscaling climatic forcing from the Hamburg GCM (ECHAM)

To derive climatic scenarios for the future, output from the Hamburg GCM (ECHAM) was used. A distinction was made between data to derive *patterns* of climatic change and data to derive *scenario's* of climatic change during the next century. The patterns of temperature and precipitation

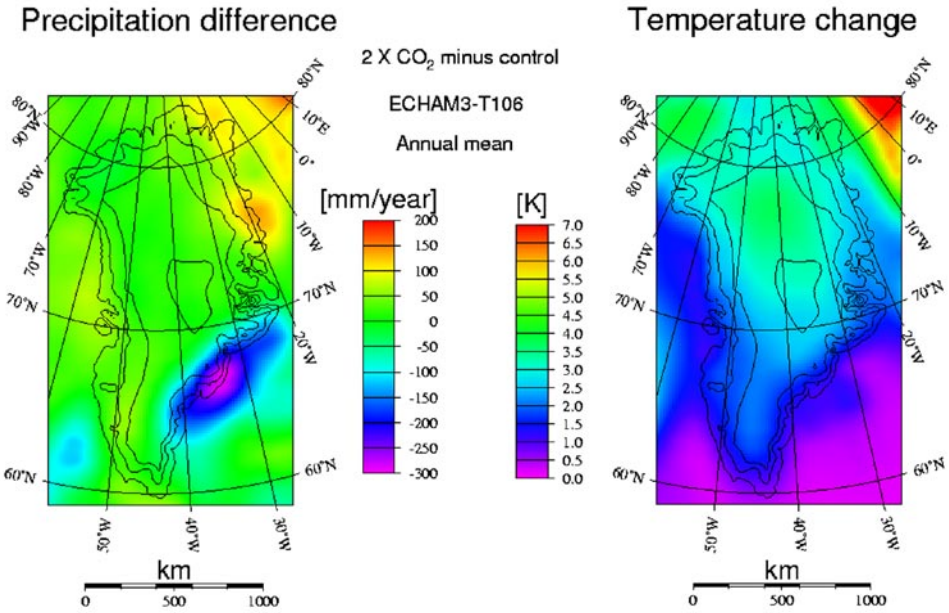

Figure 8: Annual mean temperature and precipitation changes from the ECHAM3 time-slice experiments at T106 resolution. Differences are between a $2xCO_2$ climate change run and a $1xCO_2$ control run with boundary conditions derived from a transient ECHAM1-LSG experiment at T21 resolution.

change originated from the ECHAM3 time-slice experiments at T106 resolution (Ohmura et al., 1996). This resolution corresponds to a horizontal grid of about 1.125° x 1.125°, and is one of the few of its kind presently available. Results were obtained for a present-day control run and a simulation under doubled carbon dioxide conditions. The boundary conditions (SST and sea-ice) for

these time-slice simulations were provided by the transient ECHAM1-LSG experiment at T21 resolution (Cubasch et al., 1992), respectively for observed conditions in the mid-1980's (control run) and at the time of CO_2 doubling (the decade 2040-2050). This transient experiment ran from 1985 to 2084 and was forced by the IPCC scenario A ('Business as usual'), yielding an equivalent CO_2 rise by a factor 3 after 100 years. For consistence, the same T21 run also served to derive the time-dependent scenario's over the Greenland ice sheet.

To eliminate systematic errors and minimize the effects of the still rather coarse resolution of the climate model, all climatic changes were considered in the perturbation mode. That is necessary because the absolute GCM climate data differ from the observations and because the ice-sheet margin, where the run-off takes place, is generally narrower than the model resolution, even at a T106 resolution. Also a considerable drift was observed over the ice sheets in the T21 control simulation, requiring to consider climate perturbations at the same instant in time between the climatic change run and the control run. To transfer climatic changes from the GCM to the ice-sheet model, the following procedures were adopted:

Temperature:

- Patterns of temperature change were constructed by interpolating monthly temperature differences (climatic change minus control) from the respective ECHAM3/ T106 experiments on the 20 km grid of the ice-sheet model (Fig. 8).
- The time-dependent forcing was obtained from spatially averaged monthly temperature changes (climatic change minus control for the same time instant) from the ECHAM1-LSG/ T21 simulation over the entire Greenland ice sheet for the period between 1985 and 2084.
- A scaling factor $\alpha(t)$ was constructed as the ratio of the temperature difference at time t and the mean temperature difference for the decade 2040-2050, both for the T21 data.
- The monthly T106 patterns of temperature change at time t were obtained by multiplying the 2040-2050 T106 patterns by the respective $\alpha(t)$. Fig. 9 shows the resulting average yearly temperature change over Greenland for the period 1985-2084.
- The time-dependent patterns of temperature change were superimposed on a parameterisation of surface temperature so that both the effects of changing ice-sheet elevation and background temperature change can have an effect on the surface temperature.

Precipitation:

- Patterns of precipitation change were derived by interpolating yearly precipitation ratios (climatic change divided by control) from the respective ECHAM3/ T106 experiments on the 20 km grid of the ice-sheet model (Fig. 8). A division in monthly values was in this case not meaningful because reliable information on the distribution of precipitation during the year does not exist.
- The time-dependent forcing was obtained from spatially averaged yearly precipitation ratios (climatic change divided by control for the same time instant) from the ECHAM1-LSG/ T21 simulation over the Greenland ice sheet for the period between 1985 and 2084.
- A scaling factor $\beta(t)$ was constructed as the ratio of the precipitation ratio at time t to the corresponding average value for the decade 2040-2050, both for the T21 data with respect to unity.
- The yearly T106 pattern of precipitation ratio at time t was obtained by raising the 2040-2050 T106 pattern to the power $\beta(t)$. Fig. 9 shows the resulting average yearly precipitation ratio over Greenland for the period 1985-2084.

- The time-dependent patterns of precipitation ratio were multiplied with the observed precipitation distribution to obtain precipitation rates in future climates.

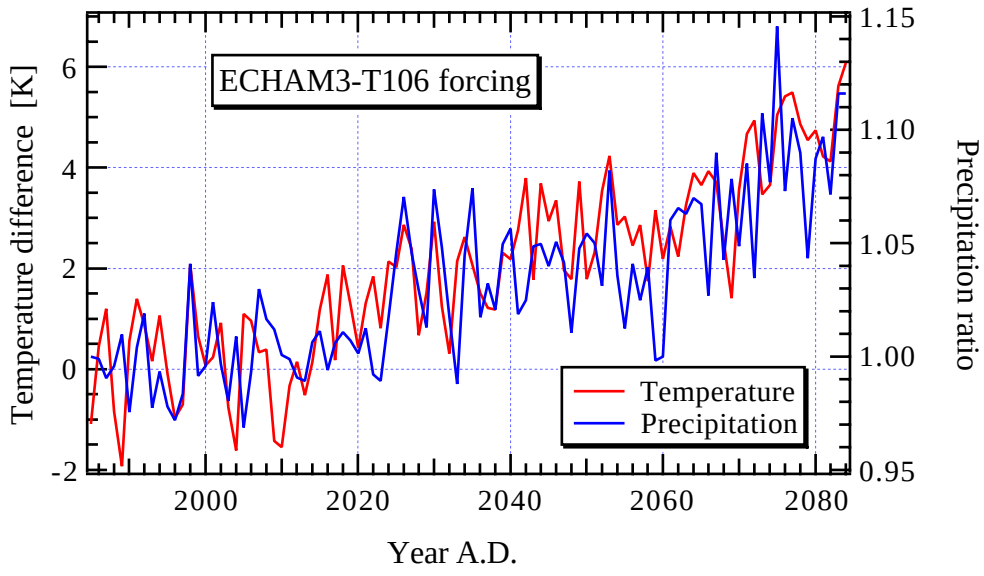

Figure 9: The ice-sheet model is forced by superimposing monthly temperature differences and yearly precipitation ratios on the best data presently available. The time-dependent results come from the ECHAM1-LSG/ T21 model run and have been scaled to comparable output over the Greenland ice sheet from the ECHAM3/ T106 run.

5.3.3. Results

Fig. 10 shows the predicted contributions to global sea-level for the period 1985 to 2084. Here, ice-volume changes were transformed into worldwide sea-level changes by assuming an ice density of 910 kg m^{-3} and a constant oceanic surface area of 3.62 x 10^8 km^2, or 71% of the Earth's surface. Interestingly, it appears that the 5 cm of sea-level rise due to changes on the Greenland ice sheet would be almost exactly balanced by changes on the Antarctic ice sheet, in spite of the fact that the Greenland ice sheet contains about 8 times less ice than the Antarctic ice sheet. That is because changes on Greenland are dominated by melting, which has a much larger sensitivity to temperature change than precipitation, which is the dominant mechanism on Antarctica where surface melting is virtually absent.

Comparing these results with those obtained in the appended paper (Huybrechts and de Wolde, in press) and those from IPCC95 (de Wolde et al., 1997) reveals that the projected sea-level changes are substantially less. The main reason is that the summer warming along the southern ice margin of Greenland, where it matters most for melting, is predicted to be only of the order of 1-2°C, which is less than the yearly average or than values higher up on the ice sheet. Also the predicted precipitation changes over Antarctica tend to be lower than what one would theoretically expect from the saturated vapour pressure, as was done in earlier analyses. However, as shown in the appended paper (Huybrechts and de Wolde, in press), the approximate balance between the two polar ice sheets only holds for the next century and only insofar changes with respect to the background evolution are concerned. Beyond the 21st century, even when assuming greenhouse gas stabilization, the Greenland ice sheet would strongly dominate the response, and even irreversibly melt down after a few thousand years, producing a eustatic sea-level rise of about 7 m.

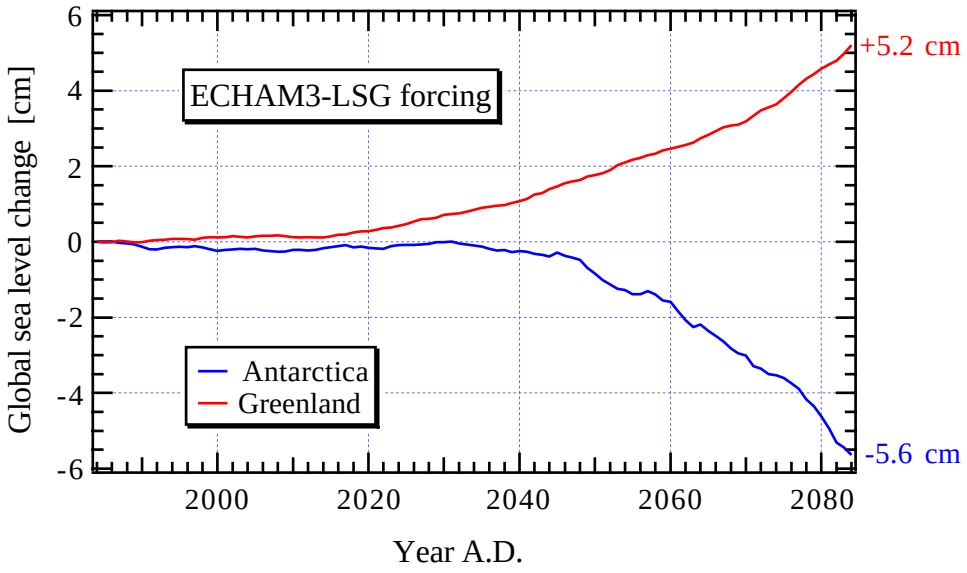

Figure 10: Predicted contribution of the Greenland ice sheet to global sea-level changes during the next century. For comparison, results are shown from a similar experiment conducted on the Antarctic ice sheet. The results do not include the background evolution due to ongoing adjustments to past climatic changes.

5.3.4. Sensitivity experiments

Two series of sensitivity experiments were performed, respectively testing the way climatic changes are imposed and investigating the role of ice dynamics on the ice sheet's response. The latter series of sensitivity experiments are described in detail in the appended paper. The main result is that even on a century time scale, Greenland ice-sheet dynamics can not be neglected and counteracts the mass-balance only response (static effect) by between 10 and 20% of the total response (Huybrechts and de Wolde, in press).

From Fig. 11, it can be seen that it does not make much difference how temperature changes are imposed on the mass-balance parameterisation, either by using monthly or yearly patterns and/ or forcing. On Greenland, the temperature effect is clearly dominant: the effect of precipitation changes only (constant temperature) makes the ice sheet grow by about 0.5 cm sea-level equivalent after 100 years.

Also imposing precipitation differences rather than precipitation ratios hardly changes the result (Fig. 12). The precipitation increase in the ECHAM climate model also turns out to be less than the often assumed 5% per degree as derived from shallow ice cores.

As a conclusion, it can be said that the incorporation of temporal and spatial patterns of climatic change as derived from high-resolution GCM's is certainly an important step forward to produce more reliable results. The general trend under increased model sophistication is towards a downward revision of estimates of sea-level rise. Similar studies with output derived from other GCM's will

have to confirm whether this result represents a robust trend or is just the consequence of the specific climate model employed here.

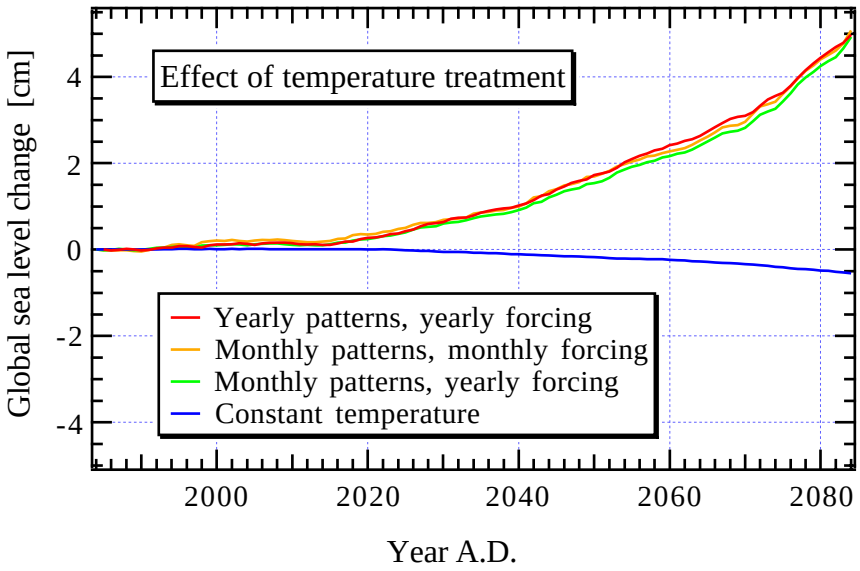

Figure 11: Dependence of the predicted sea-level change on the way temperature changes are imposed. The patterns come from T106 resolution, and the forcing from the corresponding T21 model run. Constant temperature shows the results for precipitation changes only.

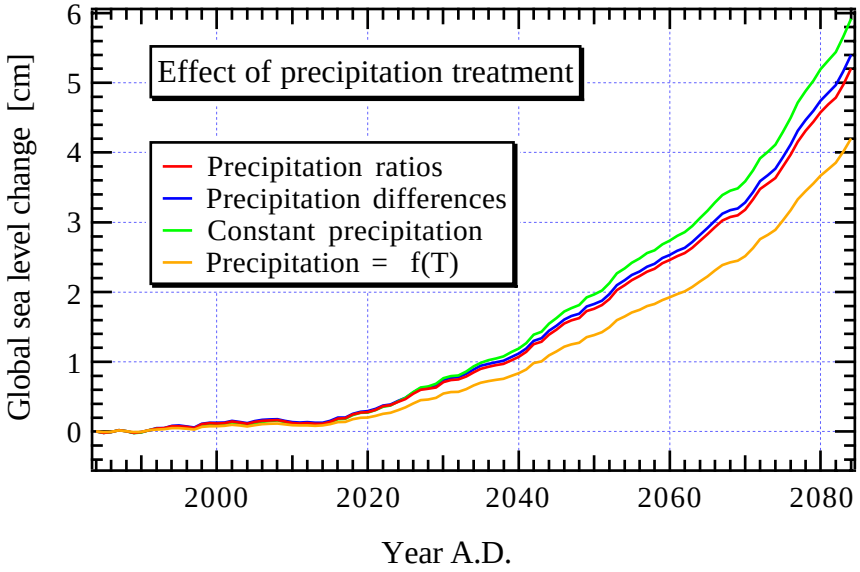

Figure 12: Dependence of the predicted sea-level change on the way precipitation changes are imposed. Constant precipitation shows the results for temperature changes only. Precipitation = f(T) assumes that precipitation rates change by 5% for every degree of yearly temperature change as done in previous studies.

6. Papers from this project

1. Huybrechts, P. (1998): Veränderungen der großen Eisschilde, in J. Lozan, H. Graßl, P. Hupfer (eds.): Warnsignal Klima/ Wissenschaftliche Fakten, Wissenschaftliche Auswertungen (Hamburg), 222-228.

2. *Huybrechts, P. and J. de Wolde (in press): The dynamic response of the Greenland and Antarctic ice sheets to multiple-century climatic warming, Journal of Climate.

3. *Huybrechts, P., and E. Le Meur (submitted): Present-day evolution patterns of ice thickness and bedrock elevation over Greenland and Antarctica, Polar Research.

4. Huybrechts, P., and C. Ritz (in preparation): A comparison of two Antarctic ice sheet models applied to the last two glacial cycles.

5. Huybrechts, P. (in preparation): Future sea-level changes from the Antarctic and Greenland ice sheets based on regionally and seasonally differentiated forcing.

6. Jung-Rothenhäusler, F. (1998): Fernerkundungs- und GIS-Studien in Nordostgrönland. Ber. Polarforschung 280, Bremerhaven, 161 pp.

7. Jung-Rothenhäusler, F., M. Schwager, J. Firestone, F. Wilhelms, H. Fisher, S. Sommer, T. Thorsteinsson, C. Mayer, S. Kipfstuhl, D. Wagenbach, P. Huybrechts, K. Zahnen, and H. Miller (submitted): Greenland accumulation distribution: a GIS based approach, Journal of Glaciology.

8. Le Meur, E., and P. Huybrechts (submitted): A computation of the gravity anomaly induced by the Greenland ice sheet: a perspective for assessing the present-day imbalance of large ice sheets? Journal of Geophysical Research.

9. *Mayer, C., F. Jung-Rothenhäusler, P. Huybrechts, and E. Le Meur (in preparation): Investigations on Nioghalvfjerdsfjorden Glacier, NE Greenland.

10. Oerter, H., Reeh, N., and Brunner, K. (1998): Storstrømmen, Northeast Greenland 1:150,000. in: IAHS/UNESCO: Fluctuation of Glaciers 1990-1995. Vol. VII, Zurich: World Glacier Monitoring Service, 63-64 + 2 map sheets.

11. Reeh, N., C. Mayer, H. Miller, H.H. Thomsen, and W. Weidick (in press): Present and past climate control on fjord glaciations in Greenland: implications for IRD-deposition in the sea, Geophysical Research Letters.

*paper included in Appendix.

7. Additional references

Bøggild, C.E., N. Reeh and H. Oerter (1994): Modelling ablation and mass-balance sensitivity to climate change of Storstrømmen, Northeast Greenland, Global and Planetary Change, 9, 79-90.

Cubasch, U., K. Hasselman, H. Hock, E. Maier-Reimer, U. Mikolajewicz, B.D. Santer, and R. Sausen (1992): Time-dependent greenhouse warming computations with a coupled ocean-atmosphere model, Climate Dynamics, 8, 55-69.

de Wolde, J. R., P. Huybrechts, J. Oerlemans, and R.S.W. van de Wal (1997): Projections of global mean sea level rise calculated with a 2D energy-balance climate model and dynamic ice sheet models. Tellus, 49A, 486-502.

Ekholm, S. (1996): A full coverage, high-resolution, topographic model of Greenland computed from a variety of digital elevation data, Journal of Geophysical Research, 101(B10), 21961-21972.

Huybrechts, P., A. Letreguilly, and N. Reeh (1991): The Greenland ice sheet and greenhouse warming. Paleogeography, Paleoclimatology, Paleoecology (Global and Planetary Change Section), 89, 399-412.

Huybrechts, P. (1994): The present evolution of the Greenland ice sheet: an assessment by modeling, Glob. and Planet. Change, 9, 39-51, 1994.

Huybrechts, P. (1996): Basal temperature conditions of the Greenland ice sheet during the glacial cycles, Annals of Glaciology, 23, 226-236.

Huybrechts, P., A.J. Payne, and the EISMINT Intercomparison Group (1996): The EISMINT benchmarks for testing ice-sheet models. Annals of Glaciology, 23, 1-12.

Huybrechts, P. (1997): Experimental description of the EISMINT grounding-line experiment, ULR: http://orca.vub.ac.be/~phuybrec/eismint/grounding.html

Le Meur, E., and P. Huybrechts (1998): Present-day uplift patterns over Greenland from a coupled ice-sheet/ visco-elastic bedrock model, Geophysical Research Letters, 25, 21, 3951-3954.

Letreguilly, A., P. Huybrechts, and N. Reeh (1991): Steady-state characteristics of the Greenland ice sheet under different climates, J. Glaciol., 37, 125, 149-157.

Mayer, C. (1996): Numerische Modellierung der Übergangszone zwischen Eisschild und Schelfeis, Berichte zur Polarforschung, 214, 150pp.

Mayer, C., and P. Huybrechts (in press): Ice-dynamic conditions across the grounding zone, Ekström ice shelf, East Antarctica, Journal of Glaciology.

Ohmura, A., M. Wild, and L. Bengtsson (1996): A possible change in mass balance of the Greenland and Antarctic ice sheets in the coming century, Journal of Climate, 9, 2124-2135.

Pfeffer, W. T., M.F. Meier, and T.H. Illangasekare (1991): Retention of Greenland runoff by refreezing: implications for projected future sea level change. J. Geophys. Res., 96, C12, 22117-22124.

Reeh, N., H. Oerter, C.E. Bøggild and F. Jung-Rothenhäusler (1994): Glaciological investigations on Storstrømmen Glacier, Northeast Greenland, in Henriksen, N. (ed.), Express Report Eastern North Greenland and Northeast Greenland 1994, Grønlands Geologiske Undersøgelske, 87-95.

Smith, W. H. F., and P. Wessel (1990): Gridding with continuous curvature splines in tension. Geophysics, 55, 3, 293-305.

Thomsen, H.H., N. Reeh, O.B. Olesen, C.E. Bøggild, W. Starzer, A. Weidick and A.K. Higgins (1997): The Nioghalvfjerdsfjorden glacier project, North-East Greenland: a study of ice sheet response to climatic change, Geology of Greenland Survey Bulletin, 176, 95-103.